The life cycle of the low salinity lenses at the surface of the Arctic Ocean

Clément Van Straaten[1], Camille Lique[2], and Nicolas Kolodziejcyk[3]

[1]Laboratoire d'Oceanographie Physique et Spatiale
[2]Laboratoire d'Océanographie Physique et Spatiale
[3]University of Western Brittany

August 19, 2024

Abstract

In the Arctic Ocean, coherent low salinity anomalies, known as lenses, and often observed at the surface and are thought to result from the input of large amount of freshwater by sea ice melting and river runoff. In this study, we analyze 20 years of a simulation performed with a high resolution ocean-sea ice regional model of the Arctic to perform a systematic detection of these lenses and track their displacements in order to gain a better understanding of their life cycle. Lenses are primarily formed during summer in response to sea ice melt, river discharge, or are associated with mesoscale eddies. They are then able to survive for weeks to months, travelling long distance across the basin as their characteristic surface salinity anomalies get eroded through vertical processes. After their formation, the lenses are associated with larger sea ice melting flux during summer, and in winter sea ice formation is intensified on top of the lenses. Over the 20-year period, the number and size of the lenses have increased over the Arctic Ocean, and the formation locations have shifted following the retreat of the sea ice edge in regions such as Greenland, Barents, and Chukchi seas. Our results suggest that these localized, intermittent and coherent lenses may be important for the large scale Arctic dynamics and the ocean-sea ice interaction.

The life cycle of the low salinity lenses at the surface of the Arctic Ocean

Clément Van Straaten[1], Camille Lique[1], Nicolas Kolodziejcyk[1]

[1]Univ Brest, CNRS, Ifremer, IRD, Laboratoire d'Océanographie Physique et Spatiale (LOPS), IUEM, F29280, Plouzané, France

Key Points:

- Surface low salinity lenses are studied in the Arctic Ocean using a Lagrangian tracking algorithm applied to an ocean-sea ice model
- Lenses are ubiquitous and primarily formed during summer due to sea ice melt, river discharge and can survive for weeks to months
- The lenses are associated with larger sea ice melting flux during summer, and in winter sea ice formation is intensified on top of them

Corresponding author: Clément Van Straaten, `clement.vanstraaten@gmail.com`

Abstract

In the Arctic Ocean, coherent low salinity anomalies, known as lenses, and often observed at the surface and are thought to result from the input of large amount of freshwater by sea ice melting and river runoff. In this study, we analyze 20 years of a simulation performed with a high resolution ocean-sea ice regional model of the Arctic to perform a systematic detection of these lenses and track their displacements in order to gain a better understanding of their life cycle. Lenses are primarily formed during summer in response to sea ice melt, river discharge, or are associated with mesoscale eddies. They are then able to survive for weeks to months, travelling long distance across the basin as their characteristic surface salinity anomalies get eroded through vertical processes. After their formation, the lenses are associated with larger sea ice melting flux during summer, and in winter sea ice formation is intensified on top of the lenses. Over the 20-year period, the number and size of the lenses have increased over the Arctic Ocean, and the formation locations have shifted following the retreat of the sea ice edge in regions such as Greenland, Barents, and Chukchi seas. Our results suggest that these localized, intermittent and coherent lenses may be important for the large scale Arctic dynamics and the ocean-sea ice interaction.

Plain Language Summary

In the cold Arctic Ocean, seawater salinity controls the ocean current and sea-ice interactions. Observations of the salinity at the surface have revealed the presence of localized and intense anomalies, referred to as lenses. As salinity measurements are scarce in the Arctic, we apply a detection and tracking algorithm to better understand the life cycle and key properties of these lenses. We show that the lenses are generally born in continental seas between April and September and die between August and April in the deep Arctic basin or outside the Arctic. Their longevity depends on their properties, such as their salinity and size, and the amount of sea ice found on top of them. The lenses also play an important role for sea-ice interaction : during summer, they concentrate the sea ice melting, while during winter, they favor the sea ice freezing above them. Over the 20 years, the number and size of lenses have increased, suggested that lenses will be more commonly found as the Arctic transitions to an seasonally ice-free state.

1 Introduction

Over the last decades, the rapid and large reduction of the Arctic sea ice cover is one of the most striking signatures of climate change in the Arctic region (IPCC, 2021). The Arctic warming amplifies the freshwater cycle, with increased precipitations and river discharge into the ocean (Bintanja, 2018). Moreover, as the Arctic transitions towards a seasonal ice cover, the melting season lengthens and the Marginal Ice Zone (MIZ) spreads drastically (Haine & Martin, 2017).

These changes of the sea ice conditions and freshwater cycle are of particular importance in the Arctic Ocean (and in the polar regions in general) as they affect the surface ocean salinity, and in these regions, the salinity primarily controls the ocean stratification and thus the ocean dynamics (Carmack, 2007). As such, gaining a better understanding of the spatial and temporal distribution of the Arctic surface salinity is of utmost importance if we are to better comprehend the functioning of the Arctic Ocean and better predict its future evolution.

During summer, sea ice melting releases a large amount of low-salinity water to the ocean surface both under sea ice and in the free ice area (Steele & Ermold, 2015). The presence of thin meltwater layers (typically a few meters depth) results in a large near-surface salinity-dominated stratification (Dewey et al., 2017). These strongly stratified layers have large impacts on the air-sea and ice-ocean interactions. For instance, it can act as a barrier between the atmosphere and the ocean surface, impeding the the momentum flux to the ocean, and the heat release from the mixed layer, thus resulting in a significant amount of solar radiation and heat trapped below the meltwater layer or the mixed layer (Smith et al., 2023). In addition, the persistence of melt lenses at the surface could locally favor the refreezing of sea ice during the following winter (Crews et al., 2022).

Despite their potential importance for the Arctic dynamics, there are only a few localized events of melt and associated low SSS signature documented and studied in the recent literature. Dewey et al. (2017) have examined the 1-D vertical dynamics of a low salinity layer close to the sea ice in the Beaufort Gyre. Supply et al. (2022) have used satellite L-Band observations of sea surface salinity (SSS) to document how sea ice melt can result in localized strong salinity anomalies (up to 5 pss) that can survive over a few weeks. In the Southern Ocean, fine scale and eddy dynamics associated with sea ice melt have been observed from gliders (e.g. Biddle & Swart, 2020). Moreover, observed low SSS anomalies are likely not solely the signature of intense sea ice melt; they can result from river runoff over the Arctic shelves (Matsuoka et al., 2016; Tarasenko et al., 2021) or they can be the SSS signature of surface eddies commonly observed in the Arctic (Cassianides et al., 2021; Kozlov et al., 2019). Contrary to the heat fluxes, the freshwater fluxes are, by nature, localized and intense, therefore they result in ubiquitous coherent and buoyant low SSS signature at the surface of the ocean.

Although some large negative SSS anomalies are commonly observed in the Arctic, we are still lacking a comprehensive picture of their importance at the scale of the Arctic basin. This would require a description of their 3-D dynamics, including their regional variability and coherence, their life cycle, their impact on sea ice melting/formation and their importance for the variations of Arctic freshwater budget on a seasonal timescale.

In this context, the objective of this study is to provide a comprehensive description of the coherent low SSS anomaly in the Arctic, and their evolution over the past 3 decades. To that aim, we will analyze outputs from a simulation performed with a high-resolution regional numerical model over 1979-2014 period, conducting a detection and a Lagrangian tracking of coherent low SSS anomalies (hereafter referred as to 'lenses') to analyze their temporal and spatial evolution and their physical parameters.

The remainder of this paper is structured as follows. Section 2 briefly presents the numerical model and simulation analyzed in this study, as well as the detection and tracking methods. In Section 3, we illustrate the life cycle of a typical single lens, before generalizing to all the lenses detected in the model outputs (Section 4). Section 5 provides a discussion of the importance of the lenses for the Arctic dynamics. Conclusions are given in Section 6.

2 Data and Methods

2.1 Numerical model and simulation

Our analysis uses a simulation performed with the high-resolution regional Arctic-North Atlantic model configuration named CREG12 (Canadian REGional; Dupont et al., 2015). It is based on the NEMO 3.6 (G. Madec and the NEMO System Team, 2016) and LIM 3.5 (Rousset et al., 2015) numerical models for the ocean and sea ice components, respectively. The configuration covers the Arctic Basin and part of the North Atlantic (down to 27°N). It has a high vertical (75 levels) and horizontal (3–4km) resolution in the Arctic Ocean, meaning that baroclinic eddies are resolved everywhere in the Arctic except on the shallow shelves (Regan et al., 2020; Meneghello et al., 2021).

Initial conditions are taken from the World Ocean Atlas 2009 climatology of temperature and salinity. The initial sea ice thickness and concentration are taken from a long global ORCA12 simulation performed by the Drakkar group (Treguier et al., 2014). Along the lateral open boundaries, monthly mean conditions (comprising 3D velocities, temperature and salinity, and sea ice thickness and concentration) taken from the same ORCA12 simulation are applied. Regarding the atmospheric forcing, we use the latest version of the Drakkar Forcing Set (DFS 5.2, which is an updated version of the forcing set described in Brodeau et al., 2010). Inputs from the river and ice sheet runoffs are taken from Hu et al. (2019) and include the large and increasing contribution from Greenland Ice Sheet melt.

The simulation covers the period from 1979 to 2014 and is described in Talandier and Lique (2021). An extended evaluation of the ocean and sea ice conditions in the Arctic Basin can be found in Regan et al. (2020) and Barton et al. (2022). In the following, we focus on the period starting in 1995 to allow for an initial spin-up of the ocean and sea ice conditions. Our analysis is based on the 5-day average outputs.

2.2 Lens definition and detection method

Our method of lens detection is solely based on their associated signature in SSS. First, we compute a climatological year by averaging the 5-day mean salinity fields for every given date over the 20 years used for our analysis. The SSS anomaly is then estimated as a difference from this climatology. An example of the SSS anomaly map obtained for February 4, 2008 is shown in Figure 1a. Second, we define a lens as a closed contour of negative SSS anomaly stronger than a given threshold. Figure 1a shows that the SSS anomaly exhibits some large spatial variations on that date, varying between -3 and 3 pss depending on the region considered. To account for the large regional variability, we choose to use a spatially variable threshold for our detection, defined as the value corresponding to the 5% quantile of the SSS distribution at each grid point over the full period. The spatially averaged threshold is around -1.8 pss, but it can reach as high as -4 pss close to the river mouths on the Arctic shelves and it is generally smaller in the Nordic Seas (Figure 1b). We have performed some sensitivity analysis to the choice of the threshold (by testing several quantile values between 1% and 25%), and found that the choice made here was allowing us to better capture the seasonal variations of the lens generation. Applying this method results in the detection of numerous lenses at each time step, with varying sizes and persistence timescales. As we are primarily interested in the long-lived coherent lenses, we further apply two criteria to eliminate the most intermittent features from our detection: we only consider (i) lenses larger than 800 km^2 (corresponding roughly to 50 grid points), and (ii) lenses surviving for at least 15 days (i.e. 3 consecutive model outputs, based on the tracking algorithm described in the following section). The smaller and most intermittent lenses are thus not considered in our analysis.

Once detected, we further assign the position of the center of the lens to the barycenter of the closed contour (Figure 1a). The properties of a given lens correspond to the average with the closed contour. To contrast the conditions within a lens and in its surrounding region, we compare the averaged properties within the lens with the average over the largest region where the lens is located. To that aim, we split up the Arctic Basin into 5 main regions roughly based on bathymetry (mainly the 500m isobath) and geographical regions (Figure 1c). The full domain used in our analysis encompasses the 5 regions and the region shown in dark grey.

2.3 Lens tracking method

To gain a deeper insight into the life cycle of the detected lenses, we develop a tracking method based on the movement of the position of the lens barycenter between two consecutive time steps. For a given lens detected at one time step, we thus search for a

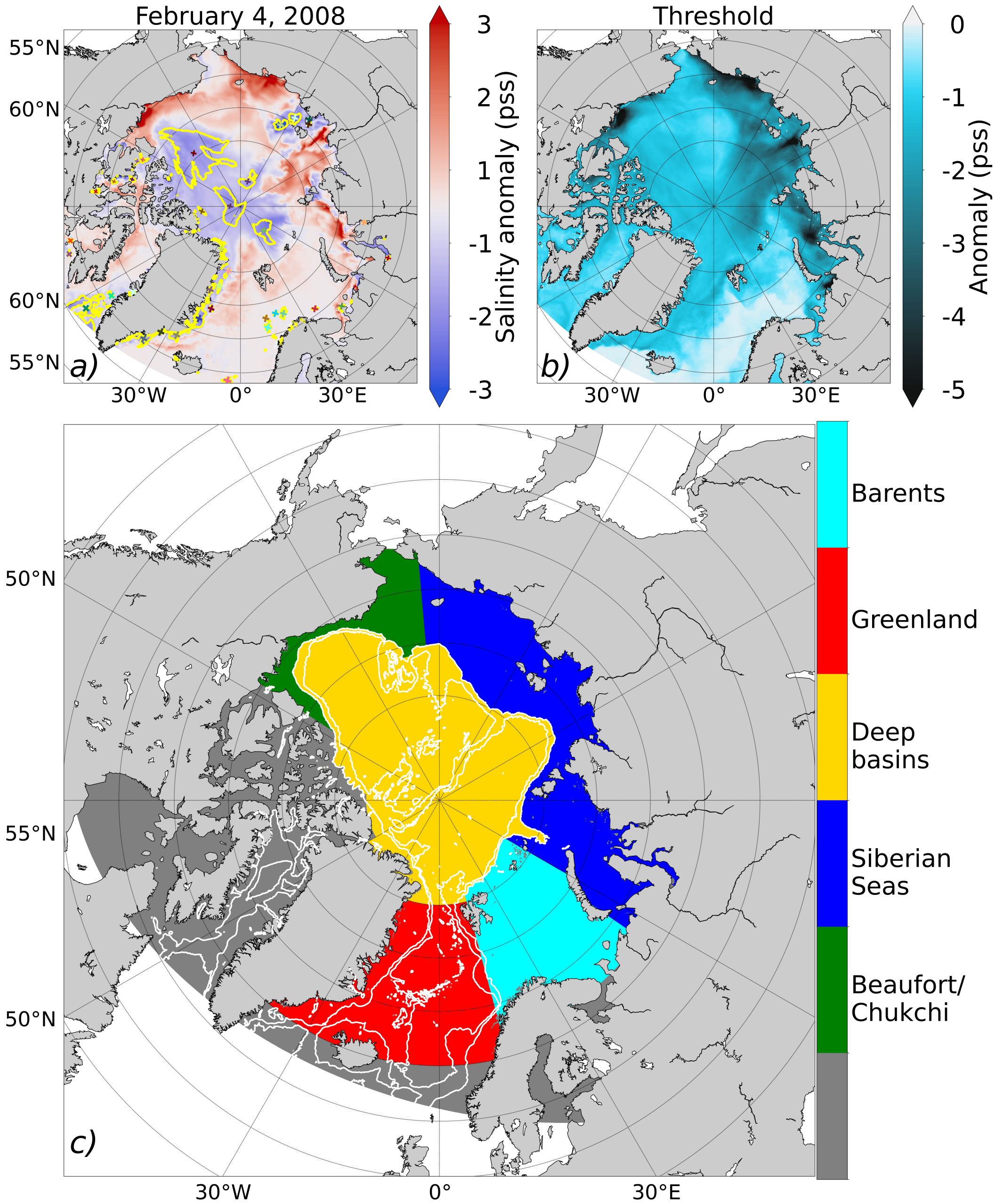

Figure 1. (a) SSS anomaly on February 4, 2008. The yellow contours delineate the detected lenses on that date, with their barycenter indicated by a colored cross. (b) Map of the SSS anomaly threshold used for the lens detection. (c) Map showing the 5 regions used in our analysis. The region shown in grey corresponds to the larger domain considered in our analysis. The white contours indicate the 500m and 2000m isobaths.

lens at the following time step with similar characteristics. Two conditions are applied to connect two lenses detected at two consecutive time steps:

- In the second time step, we search for the closest lens with a barycenter that is within 80 grid points (which is roughly 320 km) of the initial barycenter. This distance primarily corresponds to the displacement and deformation of the lenses, given their relatively slow displacement by a weak background flow (a few cm/s, or roughly 10 km over 5 days).
- We further require a minimum overlap of 10% of the grid cells between the lens detected at the two timesteps. This condition is useful to improve the tracking of the smaller lenses that do not deform much over one time step.

In some instances, the lenses can merge or split between two time steps. We thus introduce an additional categorization filter classifying lenses into three categories: merged lenses, split lenses, and new lenses. Initially, all the lenses are labeled as 'new'. In order to identify all the lenses resulting from a splitting event at a time step (t), we search for the lenses born at that time step with a center located within the contour of a lens detected at the time step (t-1). For the case with more than one lens center found within the contour, we have two options: (i) if the detected lenses at (t+1) cannot be connected to the lens detected at (t) based on the above criteria, then the new lenses are labeled as 'split'; (ii) if the properties of the lenses detected at (t+1) allow us to connect them with the lens detected at (t), then the lens with the closest center at (t+1) is assigned to be the same lens at the initial one at (t) while the other lens(es) is labeled as 'split'. To detect the merging events, we reverse the process. At a time step (t), we search for each lens if more than one lens center was found within the contour at the previous time step. The lens is thus labeled as 'merged' if that is the case.

3 Life cycle of a single lens crossing the Arctic Basin

We start by examining the case of one lens detected with our method and tracked for nearly two years by our algorithm. The lens first appears on September 22, 1996 in the Laptev Sea, where it is characterized by an SSS anomaly of up to -5.3 pss and a size of 365000 km^2 (Figure 2a, d). On November 6, 1996, it experiences a split into two lenses, after which we keep tracking the one with the center closest to the center at the previous time step. It is then advected within the transpolar drift and reaches the interior of the Eurasian Basin by August, 3 1996, where it corresponds to a local SSS anomaly larger than -2 pss (Figure 2a, d). Going forward in time, it reaches North of Greenland where it is last seen on June 19, 1998 in the form of a small closed contour (11101 km^2; Figure 2c). This means that, in total, the lens has traveled approximately 2000 km in two years, corresponding to an average advection speed of 3-3.5 km per day, which is roughly consistent with the ocean surface geostrophic velocities found in this region (Doglioni et al., 2023).

We further examine the evolution of mean properties of the conditions within the lens, that we compare with the conditions found in the largest region where the lens is located. Note that, on December 21, 1996, the lens changes the region to which it belongs (going from the Siberian Seas to the Deep Basin, see Figure 1c), inducing a discontinuity when examining the properties within and around the lens (Figure 2d-g). As it forms in September 1996, the lens is covered by thick ($\sim$ 1.5m) and concentrated ($\sim$ 90%) sea ice (Figure 2e). At the time of its formation, the surface freshwater flux from sea ice melting and freezing is positive, indicating a period of freezing. This means that the lens is not resulting from sea ice melt. Given the proximity to the mouth of the Lena river and its large freshwater discharge (Feng et al., 2021), it is likely that the lens results from the river plume advected on the shelf.

Throughout its two-year lifespan, as it is advected under sea ice, the freshwater flux within the lens, as well as the sea ice thickness and concentration within the lens, follow the large-scale seasonal cycle of the sea ice pack, with thicker and concentrated sea ice in summer and sea ice formation in winter (Figure 2d and e). It is interesting to note that there are no significant differences in sea ice-induced freshwater flux between the regions around the lens and inside the lens (Figure 2d and e), nor in sea ice conditions (except in summer 1997 when a concentration difference of 10% is visible). In contrast, sea ice is consistently thinner within the lens than the mean condition found in the Deep Basins (by about 30-80 cm).

We then look at the evolution of the temperature and salinity profiles, contrasting again the average within the lens and in the surrounding regions (Figure 2f and g). We also examine the evolution of the mixed layer depth (MLD), defined as the depth with a density difference of 0.1 kg.m^{-3} from the surface density (Peralta-Ferriz & Woodgate, 2015). As expected from the definition of a lens, the salinity within the mixed layer is fresher inside the lens, by up to 3 pss at beginning of its life. The fresher surface also results in a stronger stratification over the surface layer, and thus a thinner mixed layer, that is particularly pronounced as the lens evolves in the Deep Basins (by up to 40 m). The stronger stratification inside the lens is also associated with a warm anomaly intensified below the mixed layer, corresponding to the presence of a Near Surface Temperature Maximum (NSTM; Jackson et al., 2010).

The lens experiences a negative sea ice-induced freshwater flux between May and September 1997, corresponding to a local sea ice melt (Figure 2d). As a response, the lens gets larger, reaching about 350000 km^2 (Figure 2b and d). During that period, the MLD shoals to the surface, both in and around the lens, and the differences of salinity and temperature between the interior of the lens and its surrounding decreases to less than 2 pss and 0.1°C, respectively.

During the second year of the lens lifespan, the differences between the properties within the lens and around it become progressively smaller, although the mixed layer remains fresher inside the lens, and more heat is trapped below the mixed layer within the lens (with a temperature difference between 0.1 and 0.3°C; Figure 2g).

4 Temporal and spatial distribution of the lens field

4.1 Statistical description

Over the 1995-2014 period, we detect and track a total of 8969 lenses. Figure 3 shows the spatial distribution of the number of lens detected per box of 100 km × 100 km. Higher densities are prevalent closer to the coasts and over the continental shelves, particularly on the Siberian Shelves where it peaks at 80 lenses per 100×100 km^2. Large densities are also visible over the Greenland, Barents and Chukchi seas, while the density largely decreases in the Deep basins, and is close to zero in the Canadian Basin and around the North Pole.

We characterize the lens field by looking at the probability density functions (PDF) of some key properties of the lenses at their birth (the first time step when a lens is detected) as well as their overall age at death (Figure 4), for the different regions shown on Figure 1c. Irrespective of the region we consider, the PDF of the size at birth peaks at 800 km^2 (which is the smallest lens size captured by our detection method) and decreases rapidly when considering larger sizes, although one lens is as large as 4690000 km^2. Similarly, most of the lenses survive for 15 days (which is again the minimum possible surviving period), although some lenses can survive over longer periods. Indeed, 10% of the lenses are tracked for more than 60 days, and 2.5% for more than 105 days. We also examine the PDF of the mean salinity anomaly (compared to the detection threshold) averaged in the lens contour at their birth (Figure 4c). Regardless of the region con-

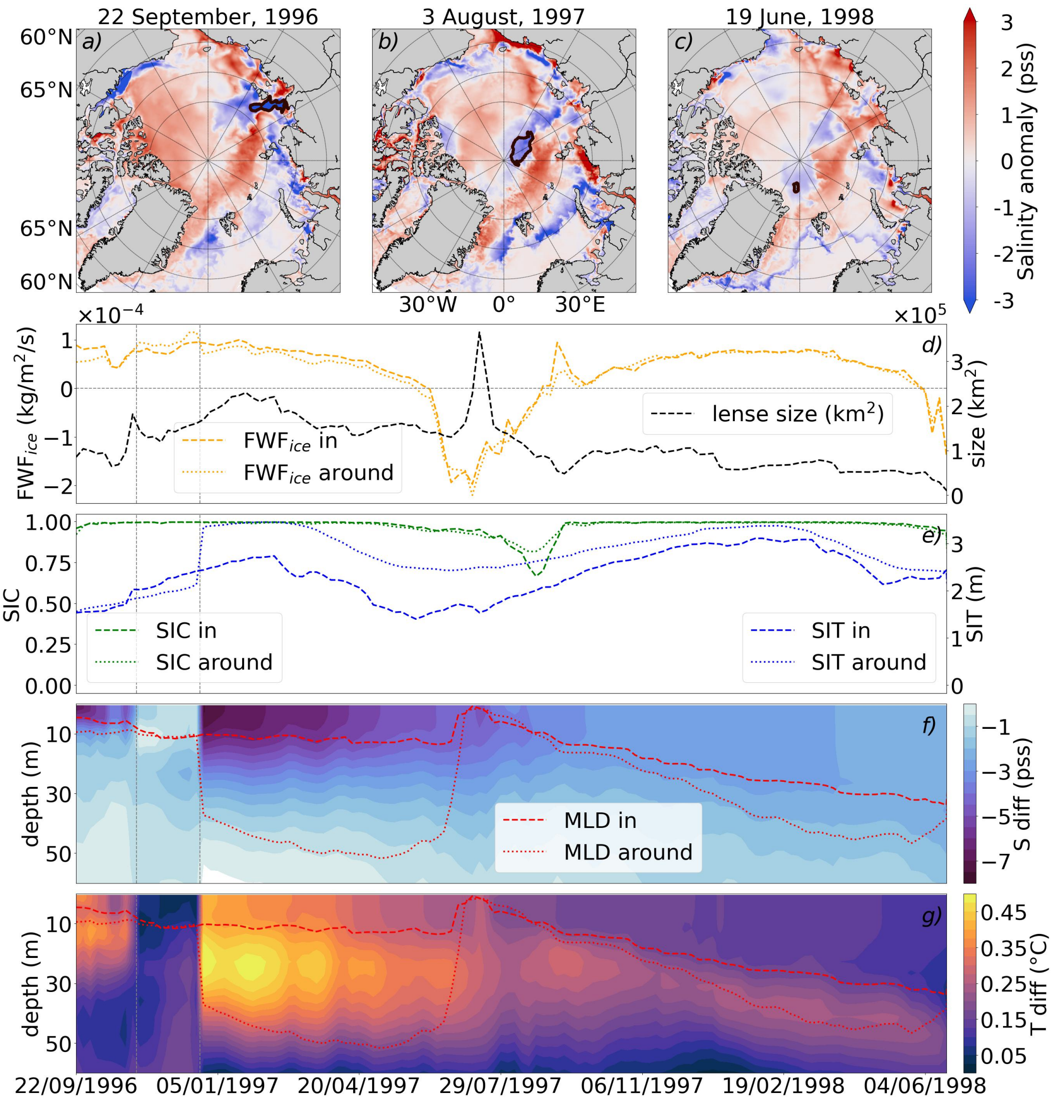

Figure 2. Maps of salinity anomalies on (a) September 22, 1996; (b) July 9, 1997; (c) June 19, 1998. The purple contour shows the lens analyzed in Section 3, (d) Time series of the lens size (black line; right axis) and the surface freshwater flux averaged within the lens (yellow dashed line; left axis) and over the region where the lens is detected (yellow dotted line; left axis). (e) Time series of the sea ice concentration and thickness averaged within the lens (blue and green dashed lines, respectively) and over the region where the lens is detected (blue and green dotted lines, respectively). Hovmöller diagrams of the difference of salinity (f) and temperature (g) profiles averaged within the lens minus over the region where the lens is detected. The red dashed and dotted lines indicate the mixed layer depth within the lens and over the region where the lens is detected, respectively. The first vertical grey dashed lines on panels d-g indicate the time of splitting of the lens and the second one indicates a change of region (see Figure 1c for the definition of the regions).

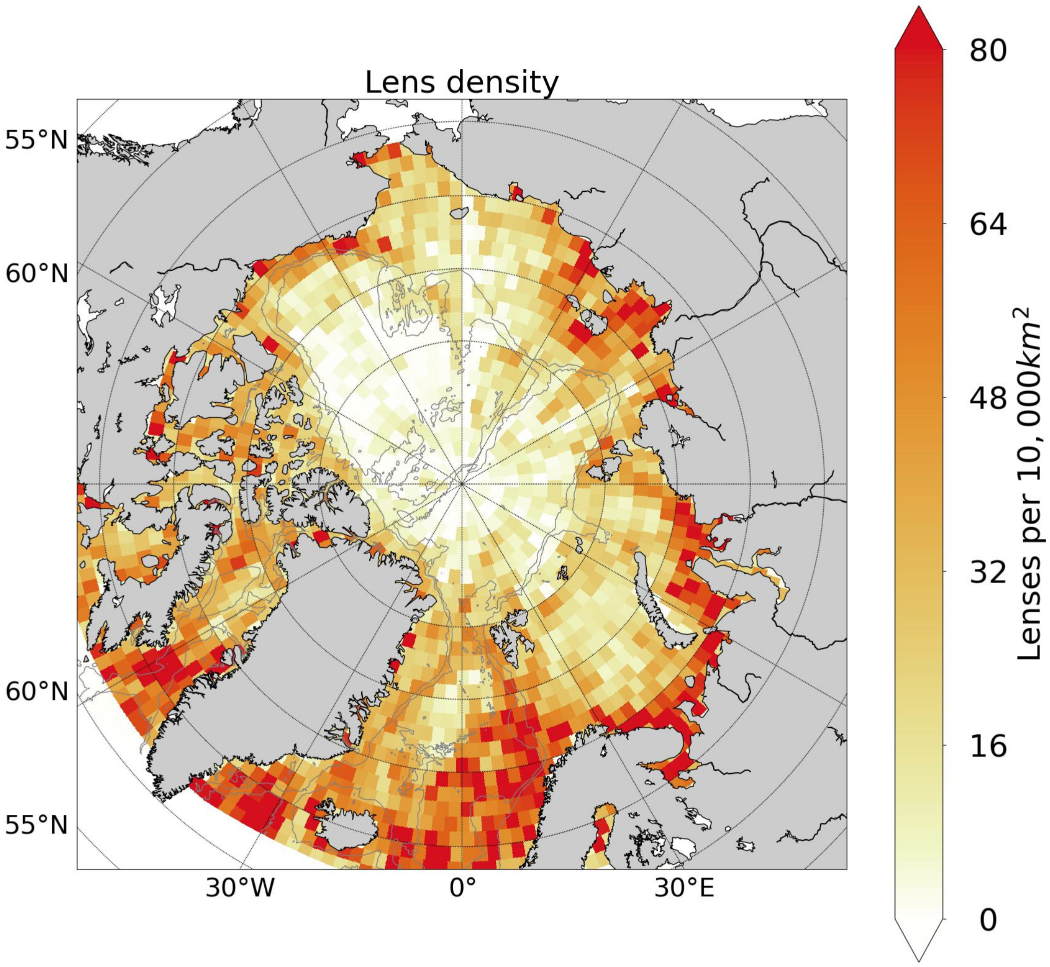

Figure 3. Spatial distribution of the density of lenses detected over the period 1995-2014, computed for boxes of 100 km × 100 km. The grey contours indicate the 500m and 2000m isobaths.

sidered, the distribution peaks in the first few salinity bin (between -0.03 pss and -0.05 pss), which accounts for between 5 and 15% of the lenses depending on the region. The distribution then gradually decreases toward larger anomalies, reaching approximately 1% for -0.5 pss. The only exception is the Siberian Seas, where the distribution peaks at -0.11 pss and 5%. Interestingly, the PDF of the mean MLD within the lenses at their birth (which corresponds roughly to the thickness of the lenses) exhibits some large differences across the regions (Figure 4d). Over the Siberian Shelves, the lens MLDs range between 0 and 10 m, and the distribution peaks between 2 and 3 m with a probability at 20%. The Barents, Chukchi, and Beaufort seas show a similar peak toward the shallow MLD, albeit less pronounced. In contrast, the PDF of the lens MLD over the Deep Basins and the Greenland Sea exhibit a very wide range of values, with no pronounced peak of the distribution. These regional differences reflect the temporal and spatial variations of the MLD across the Arctic Basin, with very shallow mixed layer depth found over the shelves in summer (Peralta-Ferriz & Woodgate, 2015; Supply et al., 2023).

It is interesting to note that we could not find a significant correlation between the different quantities discussed above. Conceptually, one may have thought that larger lenses, or lenses associated with a stronger salinity anomaly would tend to survive longer. This does not appear to be the case, suggesting that the conditions encountered by the lenses during their lifetime are more important than their initial properties to determine their ability to survive.

4.2 Seasonal variability of the lens birth and properties

As discussed in the introduction, previous studies have suggested that most of the low SSS lenses found at the surface of the Arctic Ocean are resulting from strong sea ice melt (Supply et al., 2022; Smith et al., 2023). One could thus expect a strong seasonality of the number of lens births, and possibly of the lens properties. To quantify such a seasonality, we start by coloring the positions of the centers of the lenses by their month of birth (Figure 5), considering separately the lenses categorized as new (4599 lenses), split (2545 lenses) and merged (1825 lenses). At first sight, the maps reveal that, regardless of their category, lenses can be formed throughout the year and not only during the sea ice melt season. Regions with the largest number of lens birth logically correspond to regions with the highest density of lenses (Figure 3), suggesting that lenses are most often remaining close to their birth location. These regions also correspond to regions with the largest number of split and merging events, suggesting a certain degree of randomness in the processes resulting in split and merging. Yet, a closer look also reveals that, in the Deep Basins, there are more lenses originating from a split than new ones, whereas in the Greenland Sea, there are nearly as many split lenses as new ones. This increased number of split events in these two regions is interesting as these two regions are also characterized by contrasted sea ice conditions (and hence contrasted momentum and buoyancy surface fluxes), suggesting that split events are not directly determined by the local sea ice conditions.

To further quantify the seasonality of the lens life cycle, we estimate the number of lens births for the different regions (Figure 6a). The largest number of births occurs in the Greenland Sea (more than 1600 births), followed by the Siberian Shelf and the Barents Sea. Note that alleviating the effect of considering regions of various sizes (Figure 1c) does not modify the predominance of the Greenland Sea. Overall lenses form preferentially on the shelves rather than in the interior of the Arctic Basin. Considering all the regions, the overall picture is that the majority of births occur during spring and summer, particularly between June and August, which coincides with the sea ice melt season. Regions that are fully ice covered during winter (the Deep Basins, and the Beaufort-Chukchi and Siberian shelves) exhibit a lower number of winter births.

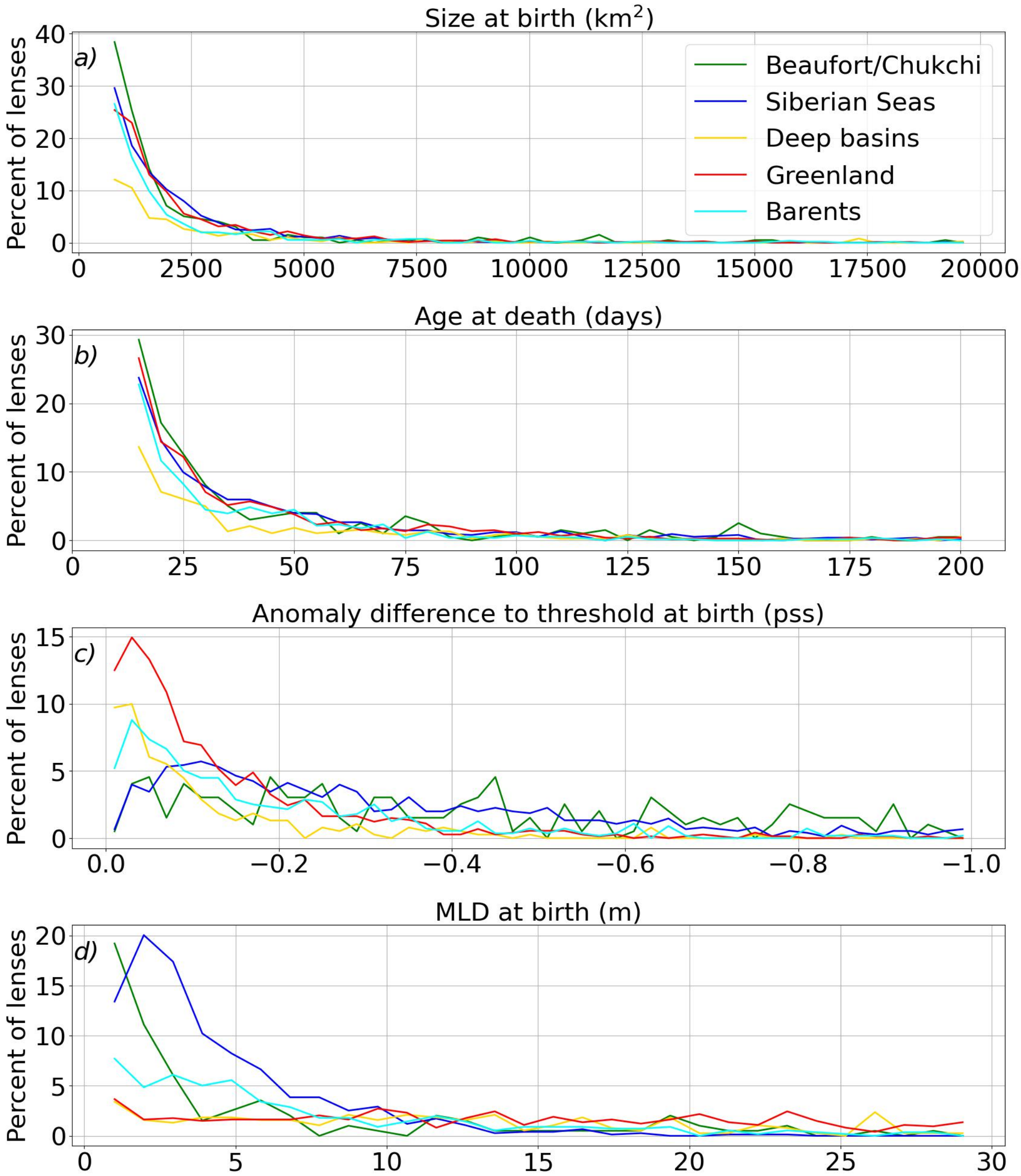

Figure 4. Probability density function per region of (a) the size of the lenses (bin size of 384 km^2); (b) the age of the lenses at their death (bin size of 5 days); (b) the difference between the salinity anomaly and the salinity threshold averaged within the lenses (bin size of 0.02 pss); (d) MLD averaged within the lenses (bin size of 1 m). Note that here we only consider the new lenses.

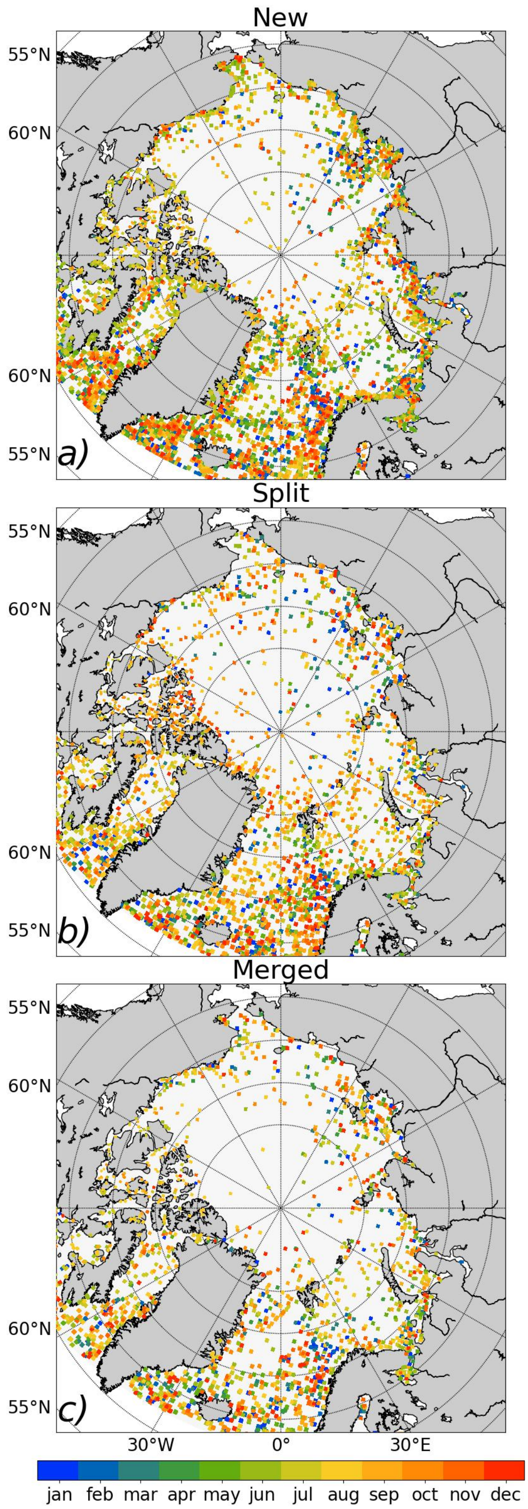

Figure 5. Maps of the position of the barycenter at their birth of each lenses classified as (a) new, (b) split and (c) merged. The colorbar indicates the month of birth.

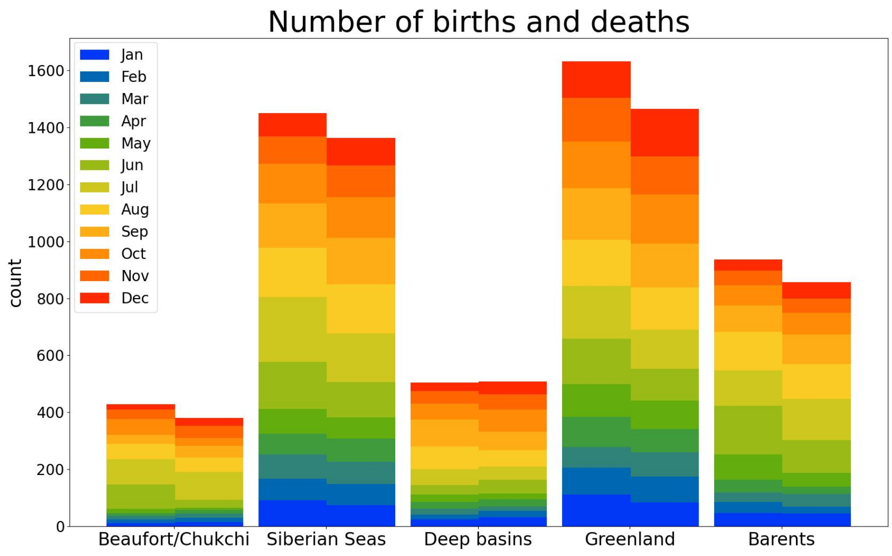

Figure 6. Number of birth and death (considering the three types of lenses) per month for the different regions. Note that 375 lenses are advected outside of the 5 regions and are thus not counted as 'dead' in a given region.

We then examine the number of lens deaths per region, that we compare to the number of births in the same region (Figure 6). For a given region, a positive unbalance between the number of births compared to the deaths suggest that a number of lenses tend to be advected outside the region. In all the regions but the Deep basins, the number of births exceed the number of deaths by about 10%. In total over the full period, 375 lenses are lost in our count, meaning that they are advected outside of the 5 discussed regions.

In the Barents, Greenland and Siberian seas, the seasonality of the deaths follow closely the seasonality of the births, with again more deaths in Summer and Fall than in Winter and Spring. In the Deep basins and the Beaufort/Chukchi seas, the seasonality of the births and deaths differs. The number of deaths in these regions outweigh the number of births during the freezing season (October to May), while the tendency reverses during the melting season. This could be due to several factors: (i) a large number of lenses advected to these regions; (ii) river runoff in these regions is small, and thus lenses there are mostly formed as a response to sea ice melt; and (iii) the presence of thicker sea ice in these regions during winter may result in a larger ocean surface stress that may enhance the dissipation (i.e. death) of the lenses.

To better explain the different life cycles of the lenses depending on their properties and the conditions found in the region where they are evolving, we now estimate the mean seasonal cycle per region of the key properties of the lenses (size, age, salinity anomaly, MLD, as well as the sea ice conditions found on top of the lenses and the differences compared to the surrounding region (Figure 7).

Comparing the seasonal cycle in the different regions, the Deep Basins stand out at first sight. There, on average, the lenses are consistently larger (up to 10^5km^2) and older (up to 250 days) than in the other regions, despite a smaller salinity anomaly (around 0.5 pss below the local threshold). The largest lenses are found in summer (July-August),

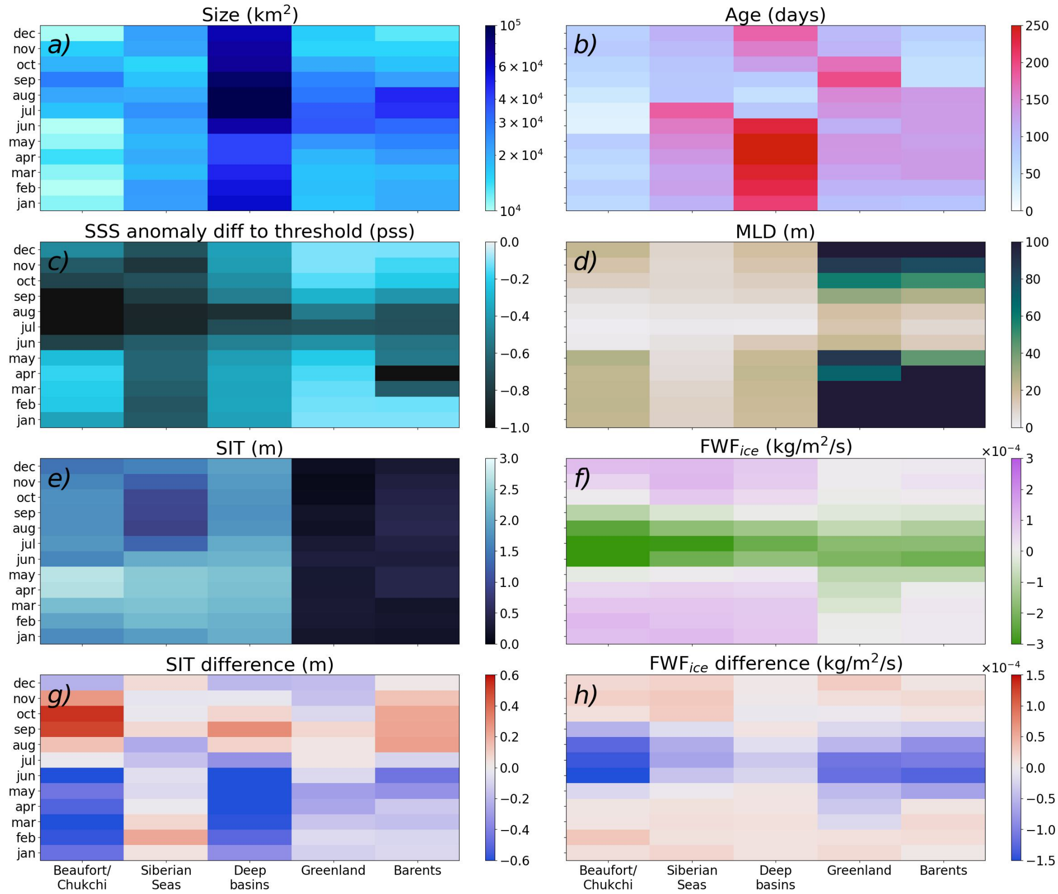

Figure 7. Monthly mean of (a) the lens sizes, (b) the lens ages, (c) the difference between the SSS anomaly averaged within each lens and the local detection threshold, (d) the MLD averaged within the lenses, (e) the sea ice thickness averaged within the lenses, (f) the freshwater flux associated with the sea ice melting and freezing averaged within the lenses, (g) and (h) the differences between the quantities shown in (e) and (f) and the average over the region where the lens is detected. Here we consider all the timesteps and thus a given lens is counted at all the timesteps it can be detected. Note that for b-d-e-f-g-h, we compute a weighted mean by considering the various sizes of the lenses.

which corresponds to the youngest lenses and the largest salinity anomaly. This suggests that, in this region, large lenses associated with strong salinity anomalies are predominantly formed in summer (Figure 6), and that the lenses tends to shrink and lose slowly their SSS signature as they evolve in the region throughout the year.

The other regions we consider exhibit a more similar behavior amongst them, and a somewhat weaker seasonality in size and age. In contrast, the mean salinity anomaly compared to the detection threshold is stronger in summer everywhere (up to -1 pss), when the lenses are predominantly formed. This suggests again that the salinity anomaly tend to erode over time.

The MLD averaged within the lenses exhibits a seasonal cycle in all the regions (Figure 7), which follows roughly the seasonality documented in the different regions of the background environment (Peralta-Ferriz & Woodgate, 2015). It is thus expected to find deeper mixed layers in the Barents and Greenland seas, where deep convection occurs during winter, and where the stratification is not solely driven by the salinity variations (Barton et al., 2022; Almeida et al., 2023). In contrast, in the ice-covered regions, where the salinity determines the density at first order, a negative salinity anomaly associated with a lens at the surface may likely result in a strengthening of the surface stratification and thus a shoaling of the mixed layer. This explains the very shallow mixed layer found in the lenses in the Deep basins, and in the Beaufort/Chukchi and Siberian seas.

In the Beaufort, Chukchi and Barents seas, sea ice tends to be thinner in winter and spring and thicker in summer and fall within the lens than in their surrounding (Figure 7e and g). The difference can reach up to 60 cm in the Beaufort/Chukchi seas in October, which represents a $\sim$ 30% difference. We acknowledge, however, that these differences may reflect both the specific behavior of the lenses and the spatial variations of the sea ice thickness across the regions, as lenses are not evenly distributed in space (Figures 3 and 6). The Barents and Greenland seas are largely ice free at least for part of the year, but the thickness differences remain substantial throughout the year. Moreover, the thickness differences have the same order of magnitude as the mean sea ice thickness within the lenses. This suggests that, in these regions, lenses could be important for the advection of sea ice or for the sea ice formation and melting.

This later idea is reinforced when looking at the freshwater flux associated with sea ice melting and freezing, averaged within the lens and in the surrounding regions (Figure 7f and h). The striking picture is that, in all the regions, the flux is strongly intensified within the lenses, with a difference that can reach as high as 50%. Consistently, there is both more melt and more freezing occurring within the lenses than in the surrounding regions. This suggests that the presences of the lenses could be important for the pan-Arctic evolution of the sea ice conditions. This is explored further in Section 5.

4.3 Interannual variability of the lens distribution

So far, we have examined the evolution of the lens field over a mean seasonal cycle built over the period 1995-2014. Yet, this period was also characterized by strong changes affecting both the ocean and sea ice conditions (Meier & Stroeve, 2022; Carmack et al., 2016), that could also affect the properties of the lens field.

Figure 8 shows a map of the birth location of the new lenses, colored this time by the year of their formation. The maps reveal that lenses are formed throughout the full period. Some regional differences are however visible. In the Greenland Sea, there seems to be more births on the western side of the basin in recent years, following roughly the position of the sea ice edge, while there are more births in the 1990s and early 2000s on the eastern side at along the Barents Sea Opening. This decreasing trend extends also over the Barents Sea, and may be related to the strong sea ice loss in this region and the shift from a β-ocean toward an α-ocean (Barton et al., 2020). In contrast, the number

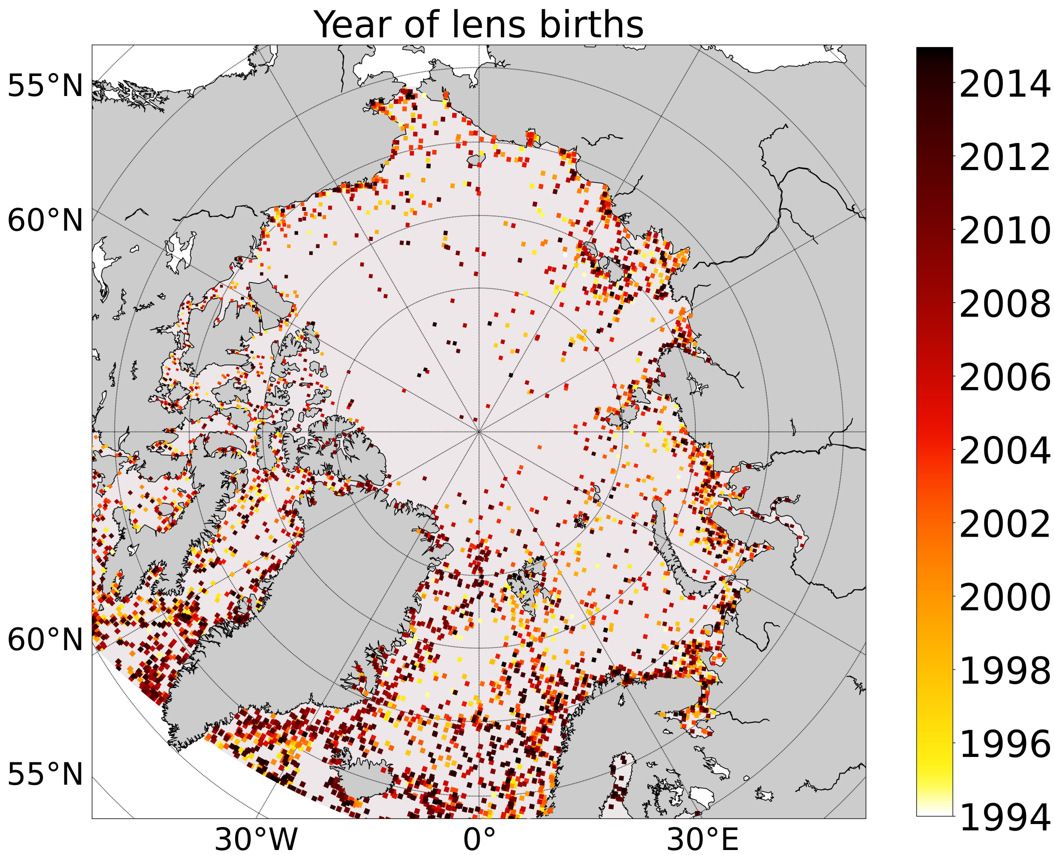

Figure 8. Maps of the position of the barycenter at their birth of all the 'new' lenses classified as (a) new, (b) split and (c) merged. The colorbar indicates the year of birth.

of births seems to increase over time in the Deep basins, and somewhat in the Beaufort/Chukchi and Siberian seas. There, a significant increase in bottom melt was reported by Perovich and Richter-Menge (2015) over the period, which may explain part of the trend.

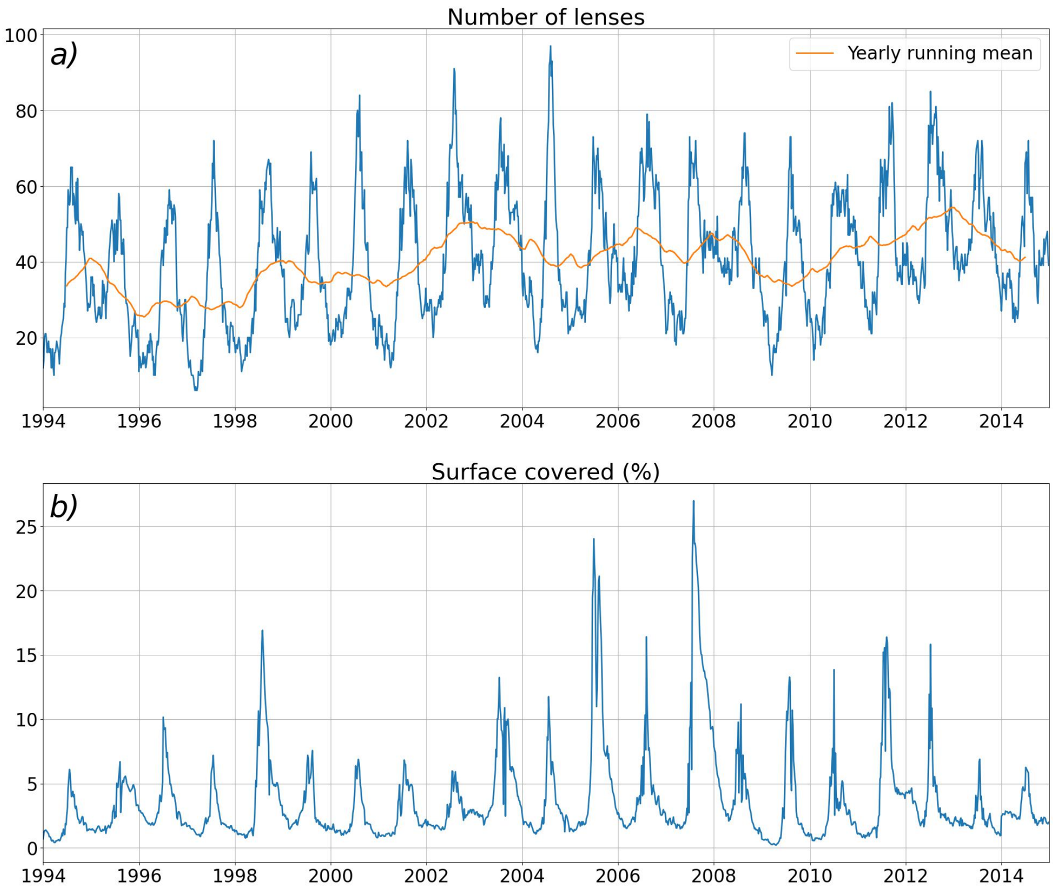

Figure 9. (a) Count of the number of lenses, at each time step over the whole domain from 1995 to 2014. The orange line shows the 12-month running mean; (b) Surface covered by lenses at each time step in percent of the surface of the full domain.

Stepping away from considering only the births of new lenses, we now produce a time series of the number of lenses detected at each time step and of the corresponding surface they occupy (Figure 9).

As expected, the two timeseries exhibit a strong seasonal cycle, with a minimum in winter and spring when the lenses are only covering 2-3% of the Arctic surface. This contrasts with a peak occurring at the end of the melting season both for the number of lenses and the surface they cover (up to 20-25% of the Arctic surface some years).

Over the 21-year period, the number of lenses exhibits a small but significant increasing trend of 1 lens per year. In addition to this trend, the two times series are affected by a large interannual variability, that largely modulates the amplitude of the seasonal cycle, that varies between 30 and 70 lenses and between 5% and 25% for the number of lenses and surface they cover, respectively. It is also interesting to note that the interannual variations of the two time series are not correlated. For instance, the largest number of lenses (97 lenses) is found in summer 2004, but the surface covered by the lenses at that time is only around 12%. The largest surface covered by the lenses amounts to

27% in summer 2007, which is also a summer characterized by a record low of the Arctic sea ice extent (Giles et al., 2008). Yet, in contrast there is not marked extrema in 2012 (the year with the lowest extent ever recorded by satellite observations). This suggests that the lens occurrence is not directly determined by the amount of sea ice melt in a given year. This is discussed in more details in the following section.

5 Discussion

5.1 Processes important for the lens formation

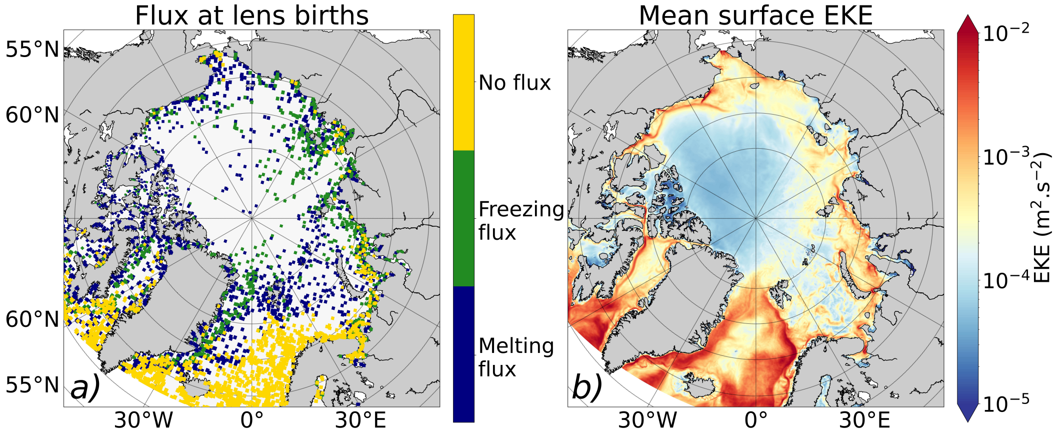

Figure 10. (a) Maps of the position of the barycenter at their birth of the new lenses clustered by the sign of their associated surface freshwater flux resulting from the the sea ice processes. (b) Surface Eddy Kinetic Energy (EKE) average over 1994-2014. Here the reference is taken as the long term mean over the full period.

To gain some further insights on the mechanism at play for the formation of the lenses, we first examine the connection between the surface forcing and the birth of the lenses. To that aim, we cluster the new lenses by the sign of the freshwater flux associated with sea ice averaged over them at their birth. A third category is added in our clustering for the new lenses with a freshwater flux equal to zero. The three clusters accounts for different parts of the total number of lenses (963, 2022 and 1614 lenses for the category corresponding to a freezing, melting and zero freshwater flux, respectively), and the clusters exhibit some clear spatial structures (Figure 10a). First, lenses with a zero surface flux are generally found at lower latitudes, and in regions that are largely ice free (e.g. the Labrador and Irminger seas, and the eastern side of the Nordic Seas). In addition, this type of lenses are also formed along the Arctic coastlines, albeit with a smaller occurrence. Second, lenses from the two other clusters (associated with either a freezing flux or a melting flux) can be found in all the regions of the Arctic, although a larger number of lenses with a melting flux are found in the Barents and Nordic seas. Many lenses are found very close to the coast, and in particular close to the river mouths. It is interesting to note that these lenses are part of the three clusters, suggesting that they are not solely formed through strong sea ice melt events. Rather, part of them are also likely derived from river runoffs, and from the river plumes that gets advected offshore keeping their low salinity signature (Matsuoka et al., 2016; Clark & Mannino, 2022). This also suggests that SSS anomalies associated to the lenses can be generated by both an intense sea ice melt, and less sea ice formation (resulting in a weak brine rejection and thus a low SSS).

Last, we note that there is a striking similarity between the regions associated with high levels of Eddy Kinetic Energy (EKE) at the surface, and the regions with a higher number of lens births (Figure 10b). This similarity is even stronger when considering the lenses that are not associated with any sea ice melt or freezing, but also all along the East Greenland Current. Without fully investigating the spatial collocations between eddies and lenses, the EKE map suggests that part of the lenses could coincide with negative SSS anomalies associated with the passage of eddies.

5.2 Lens contribution to the Arctic freshwater flux and budget

The clustering performed above reveals that 65% of the new lens birth are associated with sea ice processes. Moreover, as they evolved through time, lenses are associated with significant differences in sea ice thickness and surface freshwater flux compared to the regions where they are found (Figure 7g,h). To gain some insights on the contribution of all the lenses to the Arctic freshwater budget, we estimate the cumulated freshwater flux due to sea ice melt and freezing occurring within the lenses, that we compare to the total sea ice melt and freezing over the full domain (Figure 11). We choose to show the melting and freezing independently as, during winter, both sea ice melt and formation can happen depending on the location we consider. Overall, the amount of freshwater due to sea ice formation within the lenses remain small compared to the total (5% at most). In contrast, a significant part of the total freshwater flux associated with sea ice melt occurs with the lenses. The lens contribution reaches at least 20% every summer and peaks as high as 50% during summers 2005 and 2007. This is much larger than the surface covered by the lenses (Figure 9b) although the two numbers are not directly comparable as the total surface is computed for the full domain and not only for the ice-covered region. Yet, Figure 11 suggests that a significant part of the ice melt occurs in the form of lenses at the Arctic Ocean.

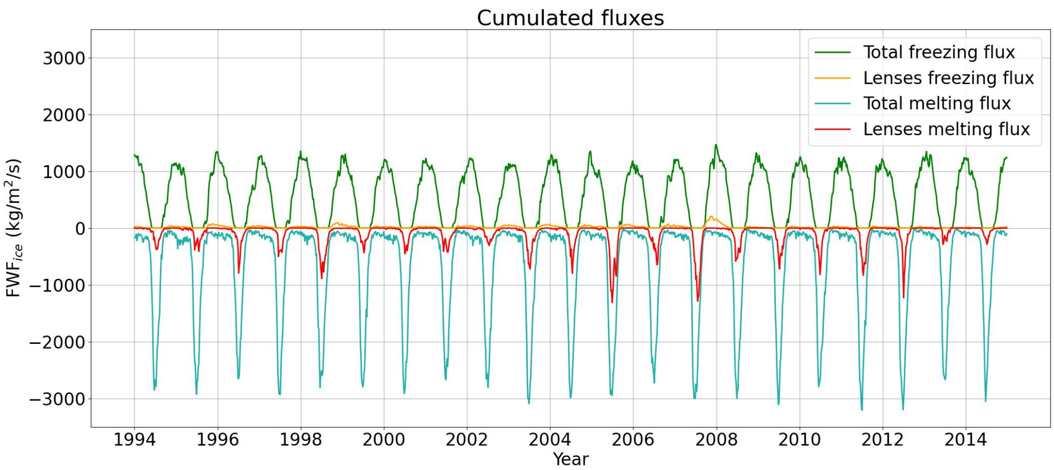

Figure 11. Time series of the freshwater flux associated with the total sea ice freezing (green) and melt (blue) compared to the same fluxes computed within the lenses (freezing in orange, melt in red).

6 Summary and Conclusions

In the Arctic Basin, the ocean surface is affected by numerous types of forcing capable of strongly modulating the SSS, including sea ice melting and freezing as well as large and localized river discharges. As a result, low SSS anomalies are generated. In the literature, these anomalies are often referred to as meltwater layers (Smith et al., 2023) or meltwater lenses (Supply et al., 2022), as only the SSS anomalies resulting from intense and localized sea ice melt were considered previously. Here, we expand these analyses by considering any low salinity coherent anomaly found at the Arctic surface, regardless of their origin.

Based on the analysis of simulation outputs from a high resolution Arctic ocean-sea ice model, we have performed a systematic detection of these lenses and have tracked their displacements in order to gain a better understanding of their life cycle. Over the period 1994-2014, we are able to detect and track a total of 8969 lenses, that are found largely along the high Arctic coastlines and in the Nordic, Irminger and Labrador seas. Most of the lenses are formed in summer (June-August), although we detect some births throughout the year, and they can survive for several months and be advected away from the birth location with the background flow. This is consistent with the characteristics of the lenses observed in summer during the MOSAIC expedition (Smith et al., 2023), that were able to survive for weeks to months. In our simulation, lenses and their associated salinity anomalies are confined to the shallow mixed layer which is often less than 5m deep. Lenses are associated with SSS anomalies of up to 3 pss compared to a mean climatological year. This characteristics values of the lenses suggest that our model tend to simulate weaker anomalies, that are less confined to the surface than the lenses observed by Smith et al. (2023). This is likely resulting from the model vertical mixing scheme (Blanke & Delecluse, 1993), that tends to diffuse over the mixed layer any surface anomalies rather than maintaining strong gradient within the mixed layer. Yet, the model is able to capture the formation of a near surface temperature maximum that tends to appear below the mixed layer and tend to trap a significant amount of heat and can survive for a several months and potentially modulate any future sea ice formation (Jackson et al., 2010; Steele et al., 2011).

We further find some strong connections between the lenses and sea ice. First, 65% of the lenses are generated by either some strong sea ice melt, or by less than usual sea ice formation (that results in a negative SSS anomaly compared to the climatology). Second, throughout their life cycle, lenses are on average associated by a local anomaly of the sea ice thickness and they lenses consistently encounter both more freezing during winter and more melting during summer compared to their surroundings. The local anomalies are particularly noticeable in the Greenland and Barents seas, where the differences of freezing freshwater flux on top of the lenses and average over a larger region can be as high as half of the total fluxes, suggesting that sea ice formation occurs disproportionately over the lenses in these areas.

Once formed, lenses can travel over long distances. More than half of the lenses detected here experience a splitting event during their life time, and another 25% experiences a merging with one or more other lens. The examination of a few cases suggests that lenses and their associated SSS anomalies tend to be gradually eroded over time through vertical mixing, similar to what was found by Dewey et al. (2017) in the seasonal ice zone of the Beaufort Sea. Yet, future studies are required to fully quantify the importance of the different processes contributing to the lens erosion.

Overall our results suggest that these lenses mediate a significant part of the freshwater flux in the Arctic Ocean. They may thus be important for the large scale Arctic dynamics and the ocean-sea ice interplay. As the Arctic transitions toward a seasonally ice-free ocean, the increase of the river runoff and the sea ice melt (Carmack et al., 2016) as well as the possible intensification of the eddy activity (Li et al., 2024) will likely result in more frequent occurrences of these features in the future.

7 Open Research

A full description of the simulation used in this study (CREG12.L75-REF08 Canadian) as well as all the information required to produce the model output are available in open access at https://doi.org/10.5281/zenodo.5789520. It includes the configuration files, the links to boundary conditions, atmospheric forcing and initialization files.

The detection and tracking algorithms will be made available on a shared folder upon publication of the paper.

Acknowledgments

The authors were supported by funding from the CLIMArcTIC project funded by the "PPR Océan et Climat—France 2030" (contract ANR-22-POCE-0005). We acknowledge the European Space Agency's Climate Change Initiative (ESA CCI) for providing funding to develop the activities of this research under contract number 4000123663/18/I-NB, Phase 2 of the Sea Surface Salinity CCI+ R&D project, as specified in proposal reference ARG-003-130-OPT. The pan-Arctic simulation was performed using HPC resources from the French GENCI-CINES center (Grant 2018-A0050107420). We are particularly grateful to Claude Talandier who has set up the configuration and produced the simulation, and to Alexandre Supply for useful discussions at the early stage of the study.

References

Almeida, L., Kolodziejczyk, N., & Lique, C. (2023). Large scale salinity anomaly has triggered the recent decline of winter convection in the greenland sea. *Geophysical Research Letters*, *50*(21), e2023GL104766. Retrieved from `https://agupubs.onlinelibrary.wiley.com/doi/abs/10.1029/2023GL104766` (e2023GL104766 2023GL104766) doi: https://doi.org/10.1029/2023GL104766

Barton, B. I., Lique, C., & Lenn, Y.-D. (2020). Water mass properties derived from satellite observations in the Barents Sea. *Journal of Geophysical Research: Oceans*.

Barton, B. I., Lique, C., Lenn, Y.-D., & Talandier, C. (2022). An ice-ocean model study of the mid-2000s regime change in the barents sea. *Journal of Geophysical Research: Oceans*, *127*(11), e2021JC018280. Retrieved from `https://agupubs.onlinelibrary.wiley.com/doi/abs/10.1029/2021JC018280` (e2021JC018280 2021JC018280) doi: https://doi.org/10.1029/2021JC018280

Biddle, L. C., & Swart, S. (2020). The observed seasonal cycle of submesoscale processes in the antarctic marginal ice zone. *Journal of Geophysical Research: Oceans*, *125*(6), e2019JC015587. Retrieved from `https://agupubs.onlinelibrary.wiley.com/doi/abs/10.1029/2019JC015587` (e2019JC015587 10.1029/2019JC015587) doi: https://doi.org/10.1029/2019JC015587

Bintanja, R. (2018). The impact of arctic warming on increased rainfall. *Scientific reports*, *8*(1), 16001.

Blanke, B., & Delecluse, P. (1993). Variability of the Tropical Atlantic Ocean Simulated by a General Circulation Model with Two Different Mixed-Layer Physics. , *23*, 1363-1388.

Brodeau, L., Barnier, B., Penduff, T., Treguier, A. M., & Gulev, S. (2010). An ERA40-based atmospheric forcing for global ocean circulation models. *Ocean Modelling*, *31*, 88-104. doi: 10.1016/j.ocemod.2009.10.005

Carmack, E. C. (2007). The alpha/beta ocean distinction: A perspective on freshwater fluxes, convection, nutrients and productivity in high-latitude seas. *Deep Sea Research Part II: Topical Studies in Oceanography*, *54*(23-26), 2578–2598.

Carmack, E. C., Yamamoto-Kawai, M., Haine, T. W. N., Bacon, S., Bluhm, B. A., Lique, C., ... Williams, W. J. (2016). Freshwater and its role in the arctic marine system: Sources, disposition, storage, export, and physical and biogeochemical consequences in the arctic and global oceans. *Journal of Geophysical Research: Biogeosciences*, *121*(3), 675-717. Retrieved from https://agupubs.onlinelibrary.wiley.com/doi/abs/10.1002/2015JG003140 doi: https://doi.org/10.1002/2015JG003140

Cassianides, A., Lique, C., & Korosov, A. (2021). Ocean eddy signature on sar-derived sea ice drift and vorticity. *Geophysical Research Letters*, *48*(6), e2020GL092066. Retrieved from https://agupubs.onlinelibrary.wiley.com/doi/abs/10.1029/2020GL092066 (e2020GL092066 2020GL092066) doi: https://doi.org/10.1029/2020GL092066

Clark, J. B., & Mannino, A. (2022). The impacts of freshwater input and surface wind velocity on the strength and extent of a large high latitude river plume. *Frontiers in Marine Science*, *8*. Retrieved from https://www.frontiersin.org/articles/10.3389/fmars.2021.793217 doi: 10.3389/fmars.2021.793217

Crews, L., Lee, C. M., Rainville, L., & Thomson, J. (2022). Direct observations of the role of lateral advection of sea ice meltwater in the onset of autumn freeze up. *Journal of Geophysical Research: Oceans*, *127*(2), e2021JC017775. Retrieved from https://agupubs.onlinelibrary.wiley.com/doi/abs/10.1029/2021JC017775 (e2021JC017775 2021JC017775) doi: https://doi.org/10.1029/2021JC017775

Dewey, S. R., Morison, J. H., & Zhang, J. (2017). An edge-referenced surface fresh layer in the beaufort sea seasonal ice zone. *Journal of Physical Oceanography*, *47*(5), 1125 - 1144. Retrieved from https://journals.ametsoc.org/view/journals/phoc/47/5/jpo-d-16-0158.1.xml doi: https://doi.org/10.1175/JPO-D-16-0158.1

Doglioni, F., Ricker, R., Rabe, B., Barth, A., Troupin, C., & Kanzow, T. (2023). Sea surface height anomaly and geostrophic current velocity from altimetry measurements over the arctic ocean (2011–2020). *Earth System Science Data*, *15*(1), 225–263. Retrieved from https://essd.copernicus.org/articles/15/225/2023/ doi: 10.5194/essd-15-225-2023

Dupont, F., Higginson, S., Bourdallé-Badie, R., Lu, Y., Roy, F., Smith, G., ... Davidson, F. (2015). A high-resolution ocean and sea-ice modelling system for the Arctic and North Atlantic oceans. *Geoscientific Model Development*, *8*(11).

Feng, D., Gleason, C. J., Lin, P., Yang, X., Pan, M., & Ishitsuka, Y. (2021). Recent changes to arctic river discharge. *Nature Communications*, *12*(1). doi: https://doi.org/10.1038/s41467-021-27228-1

G. Madec and the NEMO System Team. (2016). *Nemo ocean engine* (Tech. Rep. No. 27). Institut Pierre-Simon Laplace (IPSL). doi: 10.5281/zenodo.1464816

Giles, K. A., Laxon, S. W., & Ridout, A. L. (2008). Circumpolar thinning of arctic sea ice following the 2007 record ice extent minimum. *Geophysical Research Letters*, *35*(22). Retrieved from https://agupubs.onlinelibrary.wiley.com/doi/abs/10.1029/2008GL035710 doi: https://doi.org/10.1029/2008GL035710

Haine, T. W., & Martin, T. (2017). The Arctic-Subarctic sea ice system is entering a seasonal regime: Implications for future Arctic amplification. *Scientific reports*, *7*(1), 1–9.

Hu, X., Myers, P. G., & Lu, Y. (2019). Pacific Water Pathway in the Arctic Ocean and Beaufort Gyre in Two Simulations With Different Horizontal Resolutions. *Journal of Geophysical Research: Oceans*, *124*(8), 6414–6432.

IPCC. (2021). Ipcc, 2021: Summary for policymakers. in: Climate change 2021: The physical science basis. contribution of working group i to the sixth assessment report of the intergovernmental panel on climate change.

Jackson, J. M., Allen, S. E., Carmack, E. C., & McLaughlin, F. A. (2010). Suspended particles in the Canada Basin from optical and bottle data, 2003-2008.

Ocean Science, *6*, 799-813. doi: 10.5194/os-6-799-2010

Kozlov, I. E., Artamonova, A. V., Manucharyan, G. E., & Kubryakov, A. A. (2019). Eddies in the western arctic ocean from spaceborne sar observations over open ocean and marginal ice zones. *Journal of Geophysical Research: Oceans*, *124*(9), 6601-6616. Retrieved from https://agupubs.onlinelibrary.wiley.com/doi/abs/10.1029/2019JC015113 doi: https://doi.org/10.1029/2019JC015113

Li, X., Wang, Q., Danilov, S., Koldunov, N., Liu, C., Müller, V., ... Jung, T. (2024). Eddy activity in the arctic ocean projected to surge in a warming world. *Nature Climate Change*, *14*(2), 156-162. doi: https://doi.org/10.1038/s41558-023-01908-w

Matsuoka, A., Babin, M., & Devred, E. (2016, 06). A new algorithm for discriminating water sources from space: A case study for the southern beaufort sea using modis ocean color and smos salinity data. *Remote Sensing of Environment*, *184*, 124-138. doi: 10.1016/j.rse.2016.05.006

Meier, W. N., & Stroeve, J. (2022, December). An updated assessment of the changing arctic sea ice cover. *Oceanography*, *35*. Retrieved from https://doi.org/10.5670/oceanog.2022.114

Meneghello, G., Marshall, J., Lique, C., Isachsen, P. E., Doddridge, E., Campin, J.-M., ... Talandier, C. (2021). Genesis and decay of mesoscale baroclinic eddies in the seasonally ice-covered interior arctic ocean. *Journal of Physical Oceanography*, *51*(1), 115–129.

Peralta-Ferriz, C., & Woodgate, R. A. (2015). Seasonal and interannual variability of pan-Arctic surface mixed layer properties from 1979 to 2012 from hydrographic data, and the dominance of stratification for multiyear mixed layer depth shoaling. *Progress in Oceanography*.

Perovich, D. K., & Richter-Menge, J. A. (2015). Regional variability in sea ice melt in a changing arctic. *Philosophical Transactions of the Royal Society A: Mathematical, Physical and Engineering Sciences*, *373*(2045), 20140165. Retrieved from https://royalsocietypublishing.org/doi/abs/10.1098/rsta.2014.0165 doi: 10.1098/rsta.2014.0165

Regan, H., Lique, C., Talandier, C., & Meneghello, G. (2020). Response of Total and Eddy Kinetic Energy to the recent spin up of the Beaufort Gyre. *Journal of Physical Oceanography*, *50*.

Rousset, C., Vancoppenolle, M., Madec, G., Fichefet, T., Flavoni, S., Barthélemy, A., ... others (2015). The Louvain-La-Neuve sea ice model LIM3. 6: global and regional capabilities. *Geoscientific Model Development*, *8*, 2991.

Smith, M. M., Angot, H., Chamberlain, E. J., Droste, E. S., Karam, S., Muilwijk, M., ... Zhan, L. (2023, 09). Thin and transient meltwater layers and false bottoms in the arctic sea ice pack—recent insights on these historically overlooked features. *Elementa: Science of the Anthropocene*, *11*(1), 00025. Retrieved from https://doi.org/10.1525/elementa.2023.00025 doi: 10.1525/elementa.2023.00025

Steele, M., & Ermold, W. (2015). Loitering of the retreating sea ice edge in the arctic seas. *Journal of Geophysical Research: Oceans*, *120*(12), 7699-7721. Retrieved from https://agupubs.onlinelibrary.wiley.com/doi/abs/10.1002/2015JC011182 doi: https://doi.org/10.1002/2015JC011182

Steele, M., Ermold, W., & Zhang, J. (2011). Modeling the formation and fate of the near-surface temperature maximum in the Canadian Basin of the Arctic Ocean. , *116*(C15), 11015. doi: 10.1029/2010JC006803

Supply, A., Boutin, J., Kolodziejczyk, N., Reverdin, G., Lique, C., Vergely, J.-L., & Perrot, X. (2022). Meltwater lenses over the chukchi and the beaufort seas during summer 2019: From in situ to synoptic view. *Journal of Geophysical Research: Oceans*, *127*(12), e2021JC018388. Retrieved from https://agupubs.onlinelibrary.wiley.com/doi/abs/10.1029/2021JC018388 (e2021JC018388 2021JC018388) doi: https://doi.org/10.1029/2021JC018388

Supply, A., Lique, C., Kolodziejczyk, N., & Talandier, C. (2023, 'aug'). Drivers of the mixed layer salinity seasonal variability in the arctic ocean. *ESS Open Archive*. Retrieved from http://dx.doi.org/10.22541/essoar.169091878.83796479/v1 doi: 10.22541/essoar.169091878.83796479/v1

Talandier, C., & Lique, C. (2021, December). *Creg025.l75-nemo_r3.6.0.* Zenodo. Retrieved from https://doi.org/10.5281/zenodo.5802028 doi: 10.5281/zenodo.5802028

Tarasenko, A., Supply, A., Kusse-Tiuz, N., Ivanov, V., Makhotin, M., Tournadre, J., ... Reverdin, G. (2021). Properties of surface water masses in the laptev and the east siberian seas in summer 2018 from in situ and satellite data. *Ocean Science*, *17*(1), 221–247. Retrieved from https://os.copernicus.org/articles/17/221/2021/ doi: 10.5194/os-17-221-2021

Treguier, A., Deshayes, J., Le Sommer, J., Lique, C., Madec, G., Penduff, T., ... Talandier, C. (2014). Meridional transport of salt in the global ocean from an eddy-resolving model. *Ocean Science*, *10*, 243–255.